

Non-perturbative effects and soft-gluon dynamics in low- p_T Drell-Yan production

D. Subotić ^{*}¹, H. Jung [†]^{2,3}, A. V. Kotikov [‡]⁴, and N. Raičević [§]¹

¹Faculty of Science and Mathematics, University of Montenegro, Podgorica, Montenegro

²University of Antwerp, Antwerp, Belgium

³II. Institut für Theoretische Physik, Universität Hamburg, Hamburg, Germany

⁴Bogoliubov Laboratory of Theoretical Physics, Joint Institute for Nuclear Research, Dubna, Russia

Abstract

The transverse-momentum spectrum of Drell-Yan lepton pairs at small p_T probes non-perturbative QCD effects, including intrinsic partonic transverse momentum and initial-state soft-gluon radiation. The novel approach, PDF2ISR, is employed to study the transverse-momentum spectrum of Drell-Yan lepton pairs in the small- $p_T(\ell\ell)$ region. This framework is particularly well suited for such investigations, as it provides a systematic treatment of the dominant non-perturbative effects and their interplay. In order to extract robust physical conclusions, a detailed analysis of the technical aspects involved in the simulation of the intrinsic transverse momenta of partons inside the proton, as well as the remnant recoil schemes, was carried out. Furthermore, different approaches for the treatment of the strong coupling at low scales were investigated and confronted with available experimental data. This comparison enabled an assessment of the sensitivity of the experimental measurements to the chosen low-scale behaviour of α_s .

^{*}dusan.sub@ucg.ac.me

[†]hannes.jung@desy.de

[‡]kotikov@theor.jinr.ru

[§]natar@ucg.ac.me

1 Introduction

The production of Drell-Yan (DY) lepton pairs at hadron colliders is a benchmark process for testing QCD factorization and parton evolution. The region of small transverse momentum of the lepton pair, $p_T(\ell\ell)$, is of particular interest, as it probes the transition between perturbative and non-perturbative QCD dynamics.

At low $p_T(\ell\ell)$, the observed transverse momentum does not originate from a single source. Instead, it arises from the combined action of two physically distinct mechanisms. The first is the *intrinsic transverse momentum* of partons inside the proton, generated at a low, non-perturbative input scale, and reflecting genuine proton structure. The second is *soft-gluon radiation*, generated during initial-state parton evolution, which builds up transverse momentum dynamically, through multiple emissions governed by the behaviour of α_s at small scales.

A realistic description of the low- p_T DY spectrum therefore requires the simultaneous inclusion of both effects. Intrinsic k_T alone provides only a baseline smearing, while on the other hand soft-gluon radiation alone cannot account for the observed width and shape of the spectrum at the lowest transverse momenta. The measured DY distributions constrain the interplay of these two contributions rather than either of them in isolation.

This interplay becomes particularly transparent when comparing transverse-momentum-dependent (TMD) approaches [1, 2], based on the Parton Branching (PB) [3, 4] method, with initial-state parton showers, constructed to be consistent with collinear parton density functions (PDFs), such as PDF2ISR [5]. In PB-TMD calculations, the intrinsic transverse momentum is introduced explicitly via a non-perturbative TMD input at a low scale, while soft gluons are treated dynamically during evolution. In the PDF2ISR approach, the same physics is realised within a Monte Carlo parton shower that follows the PDF evolution consistently and allows direct access to the treatment of soft-gluon emissions and the infrared behaviour of α_s . Once soft-gluon radiation is treated consistently in the initial state, a universal intrinsic- k_T width describes DY data over a wide range of centre-of-mass energies, as shown explicitly for the case of PB-TMDs [6, 7]. The conventional PB approach is based on the PB-TMD method implemented in the CASCADE Monte Carlo generator [8], while PDF2ISR implements the PB-based initial-state shower within PYTHIA 8 [9, 10].

In this paper we study in detail the behaviour of PDF2ISR in terms of the intrinsic- k_T distribution, the treatment of soft gluons, and especially the behaviour of α_s at small scales, in comparison to what is achieved within the PB method. The final predictions of the non-perturbative effects incorporated within PDF2ISR are validated through comparison with experimental measurements over a wide range of collision energies.

The novel aspects of this work are: (i) a recoil prescription in PDF2ISR that preserves the intrinsic transverse momentum of hard initiators and allows a direct mapping to PB-TMD inputs; (ii) a quantitative demonstration that the same intrinsic- k_T width describes DY data across energies within PDF2ISR, confirming universality; and (iii) a systematic investigation of the sensitivity of low- $p_T(\ell\ell)$ DY spectra to the infrared behaviour of α_s within an ISR-consistent Monte Carlo framework.

2 PDF2ISR and DY pair production

The PDF2ISR [5] parton shower is developed to follow the evolution of collinear and TMD parton densities. Ref. [5] shows that using the same ordering conditions, splitting-function order, and kinematic constraints as in the PDFs yields a parton shower that reproduces the same effective TMD as obtained from the TMD-PDF. For the benchmark test, the PB-NLO-2018 collinear and TMD parton densities [11] have been used.

The DGLAP evolution equation can be expressed in terms of the Sudakov form factor $\Delta_a^S(z_M, \mu^2)$ as:

$$xf_a(x, \mu^2) = \Delta_a^S(\mu^2, \mu_0^2) xf_a(x, \mu_0^2) + \sum_b \int_{\mu_0^2}^{\mu^2} \frac{dq'^2}{q'^2} \Delta_a^S(\mu^2, q'^2) \int_x^{z_M} dz \hat{P}_{ab}(\alpha_s, z) \frac{x}{z} f_b\left(\frac{x}{z}, q'^2\right). \quad (1)$$

Here, q' denotes the evolution scale, and P_{ab} are the DGLAP splitting functions describing the splitting of parton b into parton a . The Sudakov form factor is given by:

$$\Delta_a(\mu^2, \mu'^2) = \exp\left(-\sum_b \int_{\mu'^2}^{\mu^2} \frac{dq'^2}{q'^2} \int_0^{z_M} dz z P_{ba}^{(R)}(\alpha_s, z)\right). \quad (2)$$

In a backward evolution of a parton shower, the Sudakov form factor Δ_{bw} includes the parton densities:

$$\Delta_{bw}(z, \mu^2, \mu_{i-1}^2) = \exp\left(-\sum_b \int_{\mu_{i-1}^2}^{\mu^2} \frac{dq'^2}{q'^2} \int_x^{z_M} dz P_{ab}^{(R)}(\alpha_s, z) \frac{x' f_b(x', q')}{x f_a(x, q')}\right). \quad (3)$$

In order to make the parton shower in PDF2ISR consistent with the PDF, PB-NLO-2018, angular ordering is applied, along with next-to-leading order (NLO) DGLAP splitting functions and maximum longitudinal momentum fraction $z_M \rightarrow 1$.

The DY lepton-pair simulation is produced at NLO with MADGRAPH5_AMC@NLO [12], applying HERWIG 6 subtraction terms, since the parton shower follows angular ordering, as described in Ref. [13]. The collinear PB-NLO-2018 Set2 NLO parton densities are used. The procedure of matching NLO with PB has been detailed in Refs. [7, 13–15].

A good description of $p_T(\ell\ell)$ is obtained in PB using PB-NLO-2018 Set2 [7, 15, 16]. In Ref. [17], a comparison between PB and PDF2ISR was shown and very good agreement in $p_T(\ell\ell)$ was observed. Here we investigate in detail the two contributions, the intrinsic- k_T distribution and the contribution of soft gluons. In PB-NLO-2018 Set2, α_s is evaluated at a scale given by the transverse momentum of the emitted parton, which is $q_T = (1-z)q'$, and the problematic region of $q_T \leq \Lambda_{QCD}$ is avoided by applying a freezing cut. Since α_s enters both in the Sudakov form factor for evolution as well as in the one for the parton shower, the non-perturbative region of α_s becomes important and will affect the $p_T(\ell\ell)$ distribution of DY pairs.

2.1 Intrinsic- k_T distributions in PB and PDF2ISR

In PB-TMD distributions, the intrinsic- k_T distribution is introduced at the starting scale μ_0 of the evolution through a TMD distribution $\mathcal{A}_a(x, \mathbf{k}, \mu_0^2)$, with \mathbf{k} being the two-dimensional transverse-momentum vector and $k_T = |\mathbf{k}|$. This distribution is parametrised in terms of a collinear parton density at the starting scale, convoluted with an intrinsic- k_T distribution described as a Gaussian of width σ :

$$\mathcal{A}_a(x, \mathbf{k}, \mu_0^2) = f_{0,a}(x, \mu_0^2) \exp\left(-\frac{k_T^2}{2\sigma^2}\right) / (2\pi\sigma^2). \quad (4)$$

The width of the Gaussian distribution of the intrinsic k_T , σ , is related to the commonly used root-mean-square intrinsic-transverse-momentum parameter q_s via $q_s = \sqrt{2}\sigma$. In PYTHIA, the primordial transverse momentum (intrinsic k_T) of each hard-scattering initiator is generated from a two-dimensional Gaussian distribution, in close analogy to the PB input. However, there are differences in the treatment of parton momenta in the recoil-sharing step.

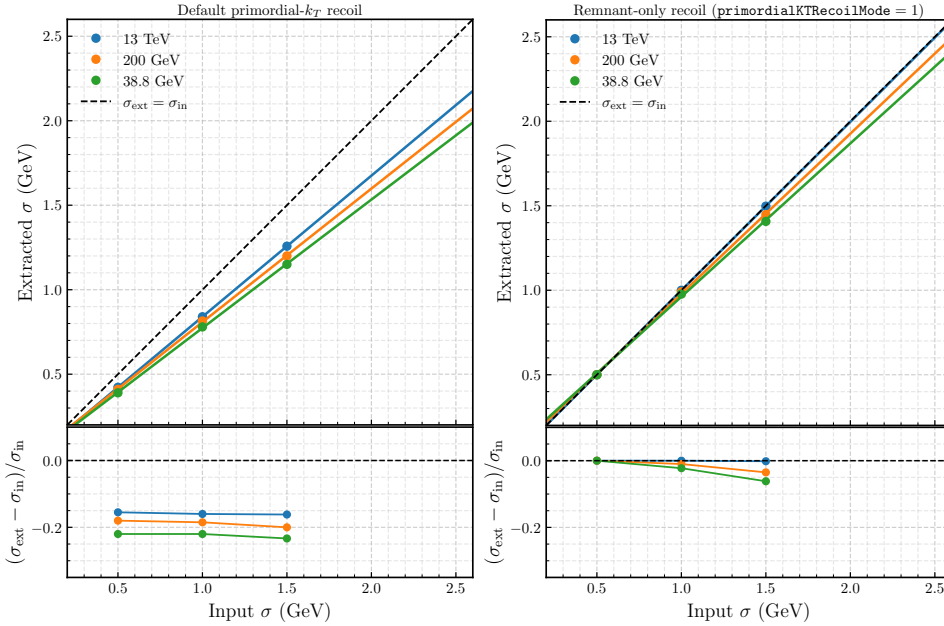


Figure 1: Comparison of input σ to the extracted one as a function of the centre-of-mass energy \sqrt{s} obtained from PYTHIA-default (left) and the modified recoil treatment (right).

In the standard PYTHIA 8 approach, a recoil-sharing step enforces exact conservation of the transverse momentum of the beam system. This compensation redistributes the net transverse momentum among all beam-related partons, including the hard initiators and beam remnants, and leads to an effective reduction of the observed intrinsic- k_T width. As a consequence, the fitted Gaussian width extracted from the incoming partons or from colour-singlet transverse-momentum spectra does not coincide with the input parameter σ . This

Table 1: Comparison of primordial- k_T recoil schemes in PYTHIA 8 and their relation to PB-TMD modelling.

	Default PYTHIA 8	Modified recoil scheme
Initiator p_x, p_y distribution	Gaussian, rescaled	Gaussian, preserved
Effective Gaussian width	$\sigma_{\text{eff}} < \sigma$	$\sigma_{\text{eff}} = \sigma$
Recoil carrier	Initiators + remnants	Remnants only
Beam- p_T conservation	Exact	Exact
Mapping to PB-TMD input	Indirect	Direct ($\sigma_{\text{PB}} = \sigma$)
Intended usage	General-purpose simulation	Theory / TMD comparison

effect is shown in the left panel of Fig. 1: a clear deviation of the extracted σ from the input σ is observed, with a mild \sqrt{s} dependence.

While this shift is not a principal issue, it makes the comparison of the intrinsic- k_T width with other approaches difficult. For comparisons with PB-TMD calculations, it is advantageous to preserve a direct and transparent relation between the input non-perturbative transverse-momentum distribution and the extracted transverse momentum. We therefore introduce a modified recoil prescription in PDF2ISR, in which the intrinsic transverse momentum of the hard initiating partons is kept exactly as generated, while the full recoil required by transverse-momentum conservation,

$$\sum_{\text{initiators}} \mathbf{k}_T + \sum_{\text{remnants}} \mathbf{k}_T = \mathbf{0}, \quad (5)$$

is absorbed exclusively by the beam remnants.

Operationally, this is achieved by modifying the recoil-sharing step in PYTHIA 8, such that the compensating transverse momentum, $\Delta \mathbf{k}_T = -\sum_{\text{initiators}} \mathbf{k}_T$, is distributed only among remnant partons, weighted by their standard recoil factors, while leaving transverse momenta of the initiators unchanged. In the PDF2ISR framework, this approach is labelled `BeamRemnants:primordialKTRecoilMode`. With this treatment, the correlation between the extracted σ and the input σ is significantly improved, as shown in the right panel of Fig. 1. A summary of the two recoil strategies is given in Tab. 1. The modified recoil prescription affects only the treatment of primordial transverse momentum and its compensation within the beam remnants. It does not rely on properties specific to Drell-Yan production and can therefore be applied equally to other final states.

In order to perform a direct comparison with PB, we have generated PB-TMD distributions with perturbative evolution, but including only intrinsic k_T for the transverse momentum, as well as distributions without any intrinsic k_T . We then compare predictions for DY production obtained with PB as implemented in CASCADE with the corresponding ones obtained with PDF2ISR, applying the same collinear PDF and the same NLO partonic calculation.

In Fig. 2, we show the DY transverse-momentum distribution for the lowest mass bin, $7 \leq m(\ell\ell) \leq 8$ GeV, for the case of intrinsic k_T only, at a low collision energy of $\sqrt{s} = 38.8$ GeV.

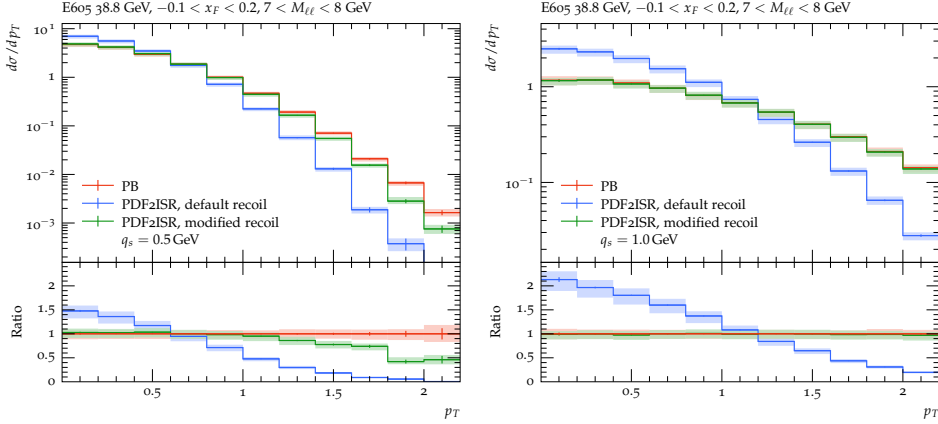


Figure 2: Comparison of $p_T(\ell)$ for the DY pairs with invariant mass $7 \leq m(\ell\ell) \leq 8$ GeV produced at $\sqrt{s} = 38.8$ GeV for two different intrinsic- k_T widths in PDF2ISR and PB (CASCADE): $q_s = 0.5$ GeV (left) and $q_s = 1.0$ GeV (right). For comparison the prediction of PDF2ISR with the default recoil scheme is shown. The uncertainty bands show the 7-point theoretical uncertainties.

(Please note that the difference at $p_T(\ell) \geq 1$ GeV for small q_s arises from matching to the NLO contribution.) For comparison, the prediction of PDF2ISR with the default recoil scheme is shown, clearly illustrating its problematic treatment. The discrepancy between the default scheme and PB increases with the value of q_s , as expected from Fig. 1.

These comparisons also demonstrate that intrinsic k_T alone only provides a baseline smearing of the transverse-momentum spectrum. The characteristic shape and normalisation of the measured $p_T(\ell)$ distribution, even at the lowest transverse momenta, require the accumulation of transverse momentum through multiple soft-gluon emissions during the initial-state evolution. Later in this section, we will explicitly verify that turning on ISR, while retaining intrinsic k_T , describes the measured low- p_T spectra accurately, underscoring that intrinsic transverse momentum cannot substitute for soft-gluon radiation.

As a further test, in Fig. 3 we compare predictions of PDF2ISR with PB when only the parton shower and TMD evolution are included, while intrinsic k_T is switched off. The comparison is shown for two cases: DY pairs with invariant mass $7 \leq m(\ell\ell) \leq 8$ GeV produced at $\sqrt{s} = 38.8$ GeV, and DY pairs in the Z -peak region produced at $\sqrt{s} = 13$ TeV. The residual differences are attributed to boost effects, since the calculation of k_T is performed in different reference frames in PDF2ISR and PB, as discussed in Ref. [5].

In the forward PB-TMD evolution, the intrinsic-transverse-momentum distribution enters via the boundary condition in eq. (4),

$$\mathcal{A}(x, \mathbf{k}, \mu_0^2) = f_0(x, \mu_0^2) G(\sigma, k_T), \quad (6)$$

with $G(\sigma, k_T) = \exp(-k_T^2/2\sigma^2)/(2\pi\sigma^2)$ a Gaussian distribution. The distribution $\mathcal{A}(x, \mathbf{k}, \mu_0^2)$

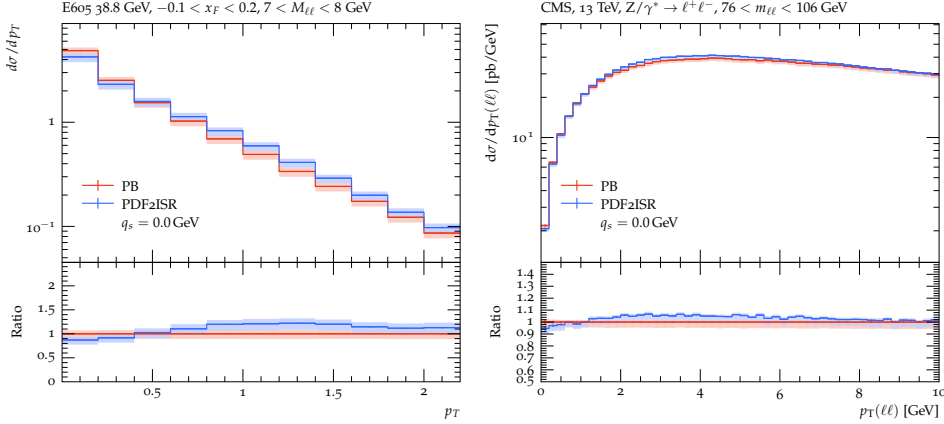


Figure 3: Comparison between PB (CASCADE) and PDF2ISR predictions obtained with parton shower and TMD evolution (without intrinsic k_T) for $p_T(\ell\ell)$ of DY pairs with invariant mass $7 \leq m(\ell\ell) \leq 8$ GeV produced at $\sqrt{s} = 38.8$ GeV (left) and for DY pairs in the Z-peak region produced at $\sqrt{s} = 13$ TeV (right). The uncertainty bands show the 7-point theoretical uncertainties.

undergoes full perturbative evolution to the scale μ :

$$\mathcal{A}(x, \mathbf{k}, \mu^2) = \Delta_a(\mu^2, \mu_0^2) \mathcal{A}(x, \mathbf{k}, \mu_0^2) + \sum_b \int \frac{d^2 \mathbf{q}'}{\pi \mathbf{q}'^2} \frac{\Delta_a(\mu^2, \mathbf{q}'^2)}{\Delta_a(\mathbf{q}'^2, \mu_0^2)} \int \frac{dz}{z} P_{ab}(z) \mathcal{A}(x', \mathbf{k}', \mathbf{q}'^2). \quad (7)$$

Here, $x' = x/z$, Δ_a denotes the PB Sudakov form factor, and \mathbf{k}' is the transverse momentum after recoil from the emission, characterised by \mathbf{q}' and z . In this formulation, the Gaussian $G(\sigma, k_T)$ is convoluted through the complete cascade of Sudakov suppressions and recoils.

In contrast, the current backward implementation in PDF2ISR constructs a parton ladder from the hard scale q down to the starting scale q_0 with $k_T = 0$ at the backward end point by construction, and only afterwards applies the intrinsic Gaussian:

$$\mathcal{A}(x, \mathbf{k}, \mu^2) = \int dx_0 \prod_{i=1}^n \left[\frac{P(z_i)}{z_i} \Delta(\mathbf{q}_i^2, \mathbf{q}_{i-1}^2) \right] f_0(x_0, \mu_0^2) G(\sigma, k_T), \quad (8)$$

where $x_0 = x / \prod_i z_i$, and the product of Sudakov factors $\Delta(q_i, q_{i-1})$ implements the no-emission probabilities along the backward chain. The intrinsic- k_T distribution, $G(\sigma, k_T)$, is thus added to the collinear parton ($k_T = 0$) at the starting scale μ_0 and does not undergo PB-style perturbative evolution. In other words, the intrinsic k_T is unevolved in the backward construction and does not experience the Sudakov suppressions and angular ordering that act on the intrinsic input in the forward PB-TMD evolution.

This difference between the forward PB-TMD evolution in eq. (7) and the current backward construction in eq. (8) is most pronounced in kinematic regions where the DY scale is close to the starting scale and the spectrum is strongly dominated by the intrinsic component, such as low \sqrt{s} and low invariant masses. In those regions, the unevolved intrinsic k_T

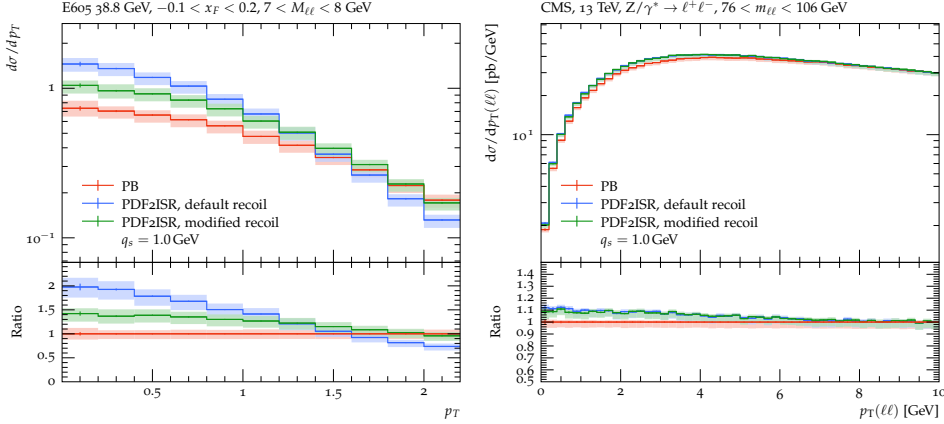


Figure 4: Comparison between PB (CASCADE) and PDF2ISR predictions obtained with an intrinsic- k_T width of $q_s = 1$ GeV and with parton shower and TMD evolution for $p_T(\ell\ell)$ of DY pairs with invariant mass $7 \leq m(\ell\ell) \leq 8$ GeV produced at $\sqrt{s} = 38.8$ GeV (left) and for DY pairs in the Z -peak region produced at $\sqrt{s} = 13$ TeV (right). For comparison the prediction of PDF2ISR with the default recoil scheme is also shown. The uncertainty bands show the 7-point theoretical uncertainties.

in the backward approach leads to noticeable deviations from the forward PB-TMD result. At high DY mass and large \sqrt{s} , where multiple soft-gluon emissions build up a substantial perturbative broadening, the details of the intrinsic treatment become less important and the agreement between backward parton-shower evolution and forward TMD evolution improves.

In particular, any extraction of q_s from a backward shower, that uses a boundary condition of the form (8), must be understood as containing a small bias. A related effect in the context of combining non-perturbative transverse momentum with TMD evolution has been discussed in Ref. [18].

Fig. 4 shows a comparison between the PB and PDF2ISR approaches for the two recoil schemes, with both non-perturbative processes simulated at $q_s = 1$ GeV. The comparison is presented for small Drell–Yan invariant masses, $7 \leq m(\ell\ell) \leq 8$ GeV, produced at $\sqrt{s} = 38.8$ GeV, and for the Z -peak region produced at $\sqrt{s} = 13$ TeV. Fig. 4 (left) shows that the overall non-perturbative contributions from PDF2ISR agree much better with the PB prediction at low energies when using the modified recoil scheme. However, a difference is still visible, which can be explained by the discussion above. Fig. 4 (right) compares the predictions at large \sqrt{s} , showing much better agreement. This confirms the argument above, that the agreement between backward parton shower evolution and the TMD evolution improves for longer evolution distances. The observed residual difference is interpreted as a systematic bias for the determination of the width of the intrinsic- k_T distribution in a backward parton shower approach.

2.2 DY data vs PDF2ISR predictions at different \sqrt{s}

After identifying and resolving a potential source of discrepancy between PDF2ISR and PB in the input value of σ for the intrinsic- k_T distribution, we now have a full understanding and control of the different aspects and impacts of intrinsic k_T . This allows us to perform detailed comparisons with measurements and to confirm that the same intrinsic- k_T value found for PB (and reported in Refs. [6, 7]) also works for PDF2ISR. This demonstrates that the intrinsic- k_T distribution can be interpreted in physical terms. For comparison with data at all \sqrt{s} , we apply $q_s = 1.04$ GeV, as obtained in Ref. [7] with the PB method.

Fig. 5 shows the prediction of the PDF2ISR approach, together with measurements of CMS [19] at the highest centre-of-mass energy, $\sqrt{s} = 13$ TeV, for the three invariant-mass bins indicated in the figure, focusing on the region of small $p_T(\ell\ell)$.

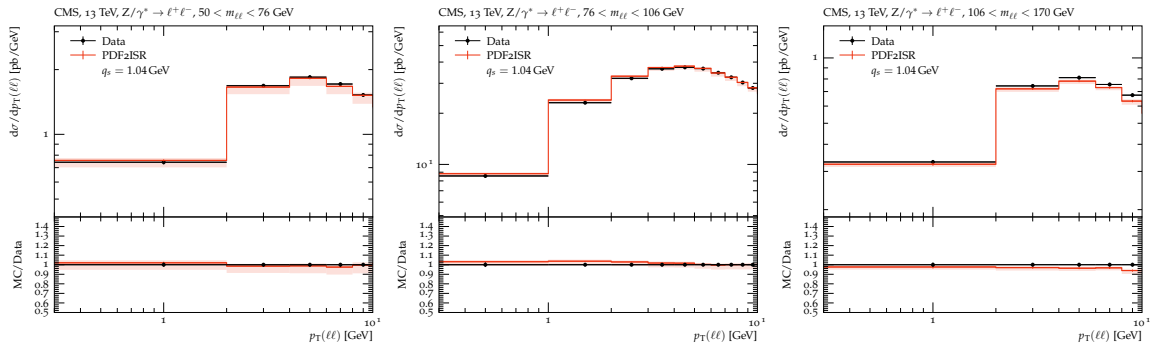


Figure 5: Transverse-momentum distributions of DY lepton pairs at $\sqrt{s} = 13$ TeV obtained with the PDF2ISR approach using PB-NLO-2018-Set2, compared to measurements [19] in three invariant-mass bins, as indicated above the histograms. The uncertainty bands show the 7-point theoretical uncertainties.

The new approach is also tested in the description of the lowest measured Drell-Yan pair transverse momenta and invariant masses, where PB provides good agreement with data [20]. In Fig. 6, the PDF2ISR predictions are compared with measurements performed at much lower energies of $\sqrt{s} = 38.8$ GeV [21] and $\sqrt{s} = 200$ GeV [22]. In addition, a comparison with Tevatron data in the Z -peak region at $\sqrt{s} = 1.96$ TeV is shown [23]. The PDF2ISR prediction provides a good description of the data down to the lowest available invariant masses and energies.

Finally, to ensure consistency, we verify whether the same q_s value as in PB provides a good fit to the measurements over a wide range of \sqrt{s} , and whether the width is independent of \sqrt{s} . For this purpose, we use the measurements shown in the previous figures. The good agreement with the data indicates that the width of the intrinsic-transverse-momentum distribution is independent of \sqrt{s} .

Following the procedure of Ref. [6], we treat the uncertainties in the same way, namely as uncorrelated, and evaluate χ^2/NDF by comparing the measurements at different centre-of-mass energies [19, 21–23] with the PDF2ISR predictions using $q_s = 1.04$ GeV.

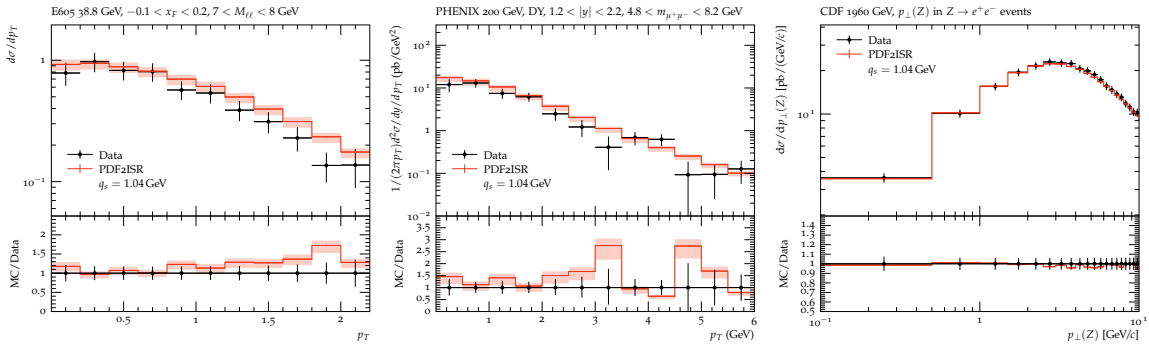


Figure 6: Transverse-momentum distributions of DY lepton pairs at $\sqrt{s} = 38.8$ GeV (left), $\sqrt{s} = 200$ GeV (middle), and $\sqrt{s} = 1.96$ TeV (right), obtained with the PDF2ISR approach using PB-NLO-2018-Set2, compared to measurements [21–23]. The invariant-mass ranges of the DY pairs are indicated above the histograms, and the uncertainty bands show the 7-point theoretical uncertainties.

The dependence of χ^2 on the centre-of-mass energy is shown in Tab. 2. As can be seen from Tab. 2, the same q_s , as determined from fits with the PB method, provides very good χ^2 values over a wide range of centre-of-mass energies.*

Table 2: Dependence of χ^2 in the non-perturbative region (as explained in the text) on the centre-of-mass energy, \sqrt{s} , obtained by comparing data at different energies [19, 21–23] with the predictions from PDF2ISR.

Experiment	\sqrt{s}	χ^2	NDF
CMS [19]	13 TeV	1.6	10
CDF [23]	1.96 TeV	5.92	14
PHENIX [22]	200 GeV	7.99	12
E605 [21]	38 GeV	5.2	11

3 The non-perturbative region in α_s

The infrared behaviour of the strong coupling α_s has been addressed in early works [24] on a dynamical, running gluon mass [25–28], as well as in the pioneering work [29] on analytic continuation of the strong coupling [30–34]. A recent review on the strong coupling is given in Ref. [35]. Latest developments have been presented in Ref. [36].

The $p_T(\ell\ell)$ distributions in DY production at small values of $p_T(\ell\ell)$ are also sensitive to

*For the LHC and Tevatron energies, the Z -peak region is used, with the emphasis placed on the low transverse-momentum region (around or below the peak of the distribution). This region corresponds to the relevant non-perturbative domain in which the ISR simulated by PDF2ISR has the largest impact.

the non-perturbative region of α_s . In PB-NLO-2018 Set2, the transverse momentum of the emitted parton, q_T , is used as the scale in α_s . Since the transverse momentum of the emitted gluon, q_T , is not restricted, because soft gluons are explicitly taken into account down to $q_0 = 0.01$ GeV, α_s has to be modified to avoid the region below the Landau pole, $q_T < \Lambda_{\text{QCD}}$.

The purpose of this study is not to determine a preferred infrared form of α_s , but to quantify how sensitive low- p_T DY observables are to the transition region between perturbative and non-perturbative scales when soft ISR is treated consistently.

In the following, we study three different approaches:

- **A: Hard Freezing:** As implemented in the default PB-NLO-2018 Set2 [11], a freezing cutoff of q_{min} was introduced, such that:

$$\alpha_s = \alpha_s(\max(q_{\text{min}}^2, \mu^2)). \quad (9)$$

The default value of the scale at which the transition from the perturbative to the non-perturbative treatment of α_s is realised is taken to be $q_{\text{min}} = 1$ GeV.

- **B: Fixed Gluon Mass:** A fixed "gluon mass" [37] $m_0 = 1$ GeV can be introduced to obtain a smooth transition:

$$\alpha_s = \alpha_s(m_0^2 + \mu^2). \quad (10)$$

- **C: Running Gluon Mass:** A "running gluon mass" [27], which depends itself on the scale μ , can be introduced:

$$\alpha_s = \alpha_s(m(\mu^2)^2 + \mu^2), \quad (11)$$

where

$$m^2(\mu^2) = \frac{m_0^2}{1 + (\mu^2/\Lambda_m^2)^\gamma}, \quad (12)$$

with $m_0 = 1$ GeV, $\Lambda_m = 0.67$ GeV, and $\gamma = 1.96$.

The parameters are chosen to best reproduce option A, which has been shown to describe DY measurements very well over a wide range of \sqrt{s} .

In Fig. 7, we show a summary of the measurements of α_s [38–58] and the different options for calculating α_s at NLO in the small- q_T region. Fig. 8 shows predictions obtained with PDF2ISR using three different ways of taming α_s in the small- $p_T(\ell\ell)$ region, compared to CMS measurements in the Z -peak region at $\sqrt{s} = 13$ TeV [19]. The predictions include theoretical uncertainties evaluated for three values of the scale $q_{\text{min}} = m_0 = 0.5, 1.0, 1.5$ GeV. The parameters used for the calculation of α_s are given above.

We observe an equally good description of the measurements with options A and C, while option B, with a fixed gluon mass taming, shows significant differences in the small- $p_T(\ell\ell)$ region. Varying the m_0 parameter in option B does not lead to an improvement.

In Fig. 9, we compare PDF2ISR predictions using different treatments of α_s to low-energy measurements of DY pairs with masses of a few GeV, produced at $\sqrt{s} = 38.8$ GeV [21] and $\sqrt{s} = 200$ GeV [22], as well as to data in the Z -peak region obtained at $\sqrt{s} = 1.96$ TeV [23].

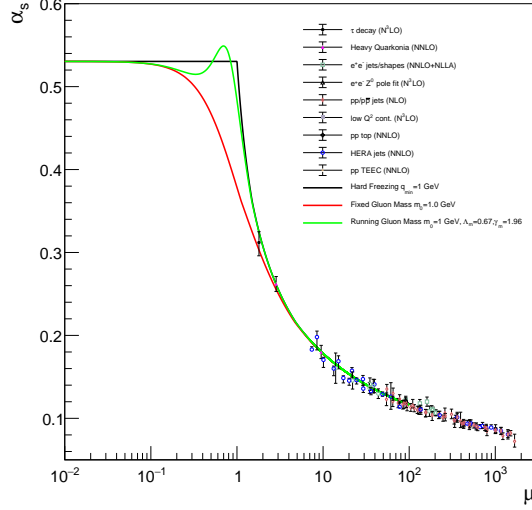


Figure 7: α_s as a function of the scale μ^2 , with experimental measurements [38–58] and predictions at NLO, for Hard Freezing (Option A), Fixed Gluon Mass (Option B), and Running Gluon Mass (Option C), with the parameters given in the text.

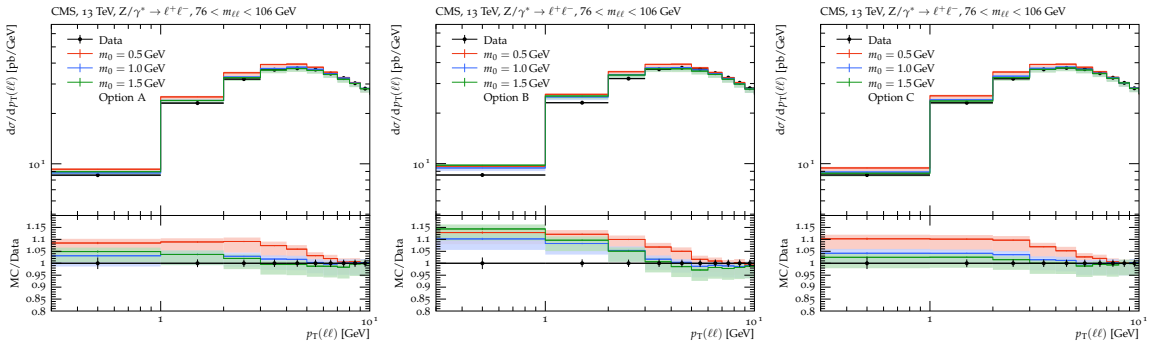


Figure 8: Transverse-momentum distributions of DY lepton pairs at $\sqrt{s} = 13$ TeV, obtained with the PDF2ISR approach, using three different ways of taming α_s and three values of the m_0 parameter, compared to measurements [19]. The uncertainty bands show the 7-point theoretical uncertainties.

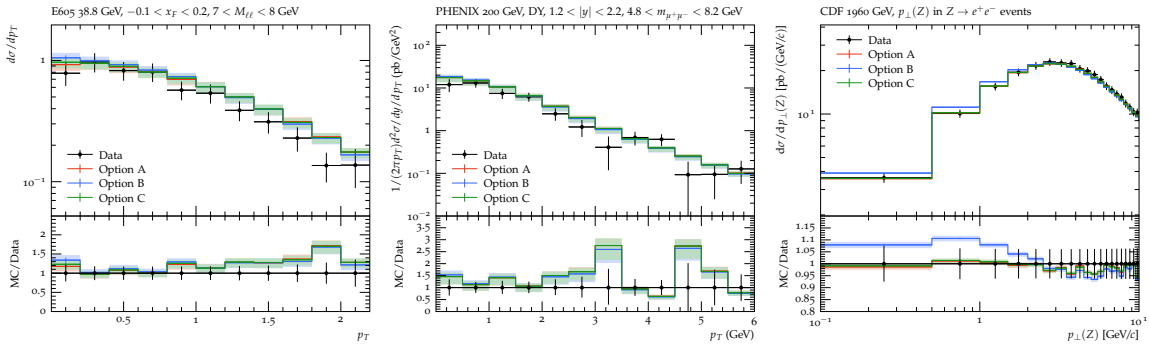


Figure 9: Transverse-momentum distributions of DY lepton pairs at $\sqrt{s} = 38.8$ GeV (left), $\sqrt{s} = 200$ GeV (middle), and $\sqrt{s} = 1.96$ TeV (right), obtained with the PDF2ISR approach, using three different ways of taming α_s with $m_0 = 1$ GeV, compared to measurements [21–23]. The invariant-mass ranges of the DY pairs are indicated above the histograms. The uncertainty bands show the 7-point theoretical uncertainties.

Due to the large experimental uncertainties of the $p_T(\ell\ell)$ measurements, as well as substantial theoretical scale uncertainties, we cannot disentangle between the different α_s options at low \sqrt{s} , while at $\sqrt{s} = 1.96$ TeV a clear difference is seen.

Returning to Fig. 8, one may argue that a somewhat larger intrinsic- k_T width could improve the agreement of option B with the LHC data. To investigate this, we examined the agreement between the PDF2ISR predictions and the CMS measurements, and found that a width of $q_s = 2.0$ GeV would provide a good description of the data in option B, as shown in the left panel of Fig. 10.

Although this value of q_s is clearly too large to represent the intrinsic transverse motion of partons inside the proton, we nevertheless examine how the PDF2ISR prediction with $q_s = 2.0$ GeV for option B performs for low DY invariant masses at small \sqrt{s} , where the spectra are much more sensitive to the intrinsic- k_T width [6]. We therefore compare option B with the measurements at $\sqrt{s} = 38$ GeV [21] for the lowest mass bin, using $q_s = 2.0$ GeV, as shown in the right panel of Fig. 10. The figure demonstrates that this choice of q_s fails to describe the data at low scales.

At this stage, we do not attempt to perform a full fit of m_0 for the different options, while pointing out the main message that the details of the turnover from the perturbative to the non-perturbative region in α_s are most relevant for the description of $p_T(\ell\ell)$ in the low- $p_T(\ell\ell)$ region at the Tevatron and the LHC. These qualitative investigations suggest that the turnover region of α_s plays the most important role for the description of $p_T(\ell\ell)$ in DY measurements, while the value of α_s in the region of $\mu \rightarrow 0$ is of lesser importance. This result is of great interest, as it shows that the DY cross section at small $p_T(\ell\ell)$ in the high-statistics Z -peak region is sensitive to the transition from the perturbative to the non-perturbative regime of α_s , and thus offers the possibility of constraining α_s in this low-scale region.

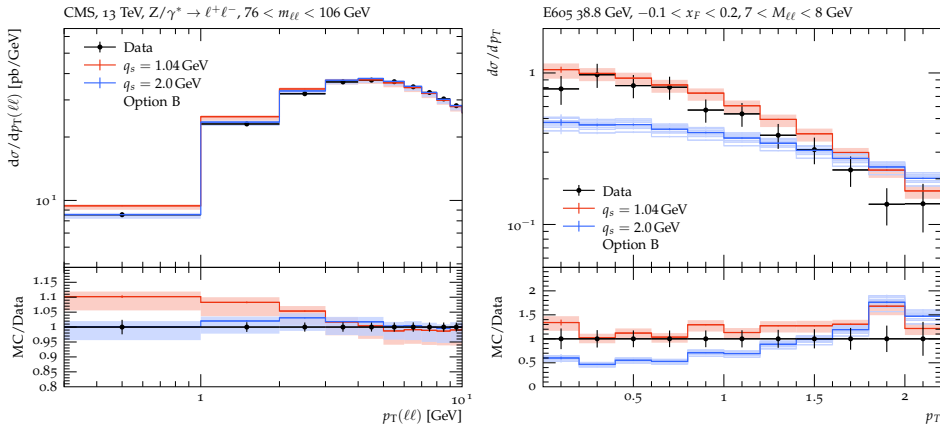


Figure 10: Transverse momentum distributions of DY lepton pairs at $\sqrt{s} = 13$ TeV (left) and $\sqrt{s} = 38.8$ GeV (right), obtained with the PDF2ISR approach, using the Fixed Gluon Mass taming (Option B), with $q_s = 2.0$ GeV, compared to measurements [19, 21]. The invariant-mass ranges of the DY pairs are indicated above the histograms. The uncertainty bands show the 7-point theoretical uncertainties.

4 Conclusion

We have applied the PDF2ISR approach to describe the non-perturbative contributions to the low- p_T region of the Drell-Yan lepton-pair spectrum. In particular, we consider the intrinsic transverse motion of partons and multiple soft-gluon emissions over a wide range of centre-of-mass energies, spanning from those covered by fixed-target experiments to those of the LHC.

The results show that PDF2ISR provides a description of the initial-state radiation contribution in the low- p_T DY region that is fully comparable to that obtained with PB-TMD calculations across a broad range of DY invariant masses and collision energies. To ensure consistency between the two approaches in describing the contribution of the intrinsic motion of partons at low transverse momentum, we performed a detailed investigation of how the treatment of parton momenta in the recoil-sharing step and the reference-frame boost affect the Drell-Yan p_T spectra. This study allowed us to disentangle technical effects from genuine physical effects that influence the non-perturbative contributions in the low- p_T DY distribution.

The remaining differences between the PYTHIA-based PDF2ISR and PB-TMD approaches originate from their distinct treatments of intrinsic transverse momentum in the presence of initial-state radiation. In the PDF2ISR approach, intrinsic k_T is introduced as a primordial, non-perturbative contribution within the backward evolution and is not dynamically evolved. In contrast, in the PB-TMD framework, transverse momentum is generated through forward evolution and thus consistently incorporates Sudakov suppression effects. Despite these conceptual differences, the PDF2ISR approach provides a description of the experimental data that is comparable in quality to that of the PB-TMD approach.

A central outcome of this study is the clear identification of the complementary roles played by intrinsic transverse momentum and soft initial-state radiation. The intrinsic- k_T distribution fixes the overall non-perturbative width of the spectrum and can be taken to be universal and energy independent at the starting scale, once soft gluons are properly included. Soft-gluon emissions generated during the initial-state evolution in turn shape the detailed behaviour of the spectrum and control the transition between perturbative and non-perturbative regions.

We further find that, within the PDF2ISR approach based on a parton shower consistent with the underlying parton densities, low- p_T Drell-Yan predictions are highly sensitive to the treatment of α_s in the transition region between perturbative and non-perturbative scales. Different infrared extensions of α_s produce visible changes in the lowest- $p_T(\ell\ell)$ bins. This indicates that intrinsic- k_T effects cannot compensate for an inaccurate modeling of soft-gluon radiation, and vice versa.

In summary, the low- p_T Drell-Yan spectrum emerges from the interplay of intrinsic parton motion and soft-gluon radiation in the initial state. Both ingredients are essential and must be treated consistently. The comparison of the PDF2ISR predictions with the conventional PB approach, as well as with experimental data, highlights the robustness of this physical picture and underlines the potential of Drell-Yan p_T measurements to constrain non-perturbative QCD dynamics and the infrared behaviour of the strong coupling. In this sense, low- p_T Drell-Yan production emerges not only as a benchmark for TMD and parton-shower formalisms, but also as a sensitive probe of the transition region of the strong coupling, complementary to traditional extractions based on event shapes and jet observables.

Acknowledgments We are grateful to D. Britzger and D. d’Enterria for providing the data point of α_s -measurements. We are grateful for many discussions with A. Bagdatova, S. Baranov, A. Lipatov, M. Malyshev, G. Lykasov and the other participants of the WeeklyOffline-Meeting during the past years. This article is part of a national scientific project that has received funding from Montenegrin Ministry of Education, Science and Innovation. The authors also acknowledge the networking support from COST Action CA24159 (SHARP).

References

- [1] R. Angeles-Martinez et al., “Transverse Momentum Dependent (TMD) parton distribution functions: status and prospects”, *Acta Phys. Polon. B* **46** (2015) 2501, arXiv:1507.05267.
- [2] R. Boussarie et al., “TMD Handbook”, *JLAB-THY-23-3780, LA-UR-21-20798, MIT-CTP/5386* (04, 2023) arXiv:2304.03302.
- [3] F. Hautmann et al., “Collinear and TMD quark and gluon densities from Parton Branching solution of QCD evolution equations”, *JHEP* **01** (2018) 070, arXiv:1708.03279.

- [4] F. Hautmann et al., “Soft-gluon resolution scale in QCD evolution equations”, *Phys. Lett. B* **772** (2017) 446, arXiv:1704.01757.
- [5] H. Jung, L. Lönnblad, M. Mendizabal, and S. Taheri Monfared, “A parton shower consistent with parton densities at LO and NLO: PDF2ISR”, *Eur. Phys. J. C* **85** (2025) 870, arXiv:2504.10243.
- [6] I. Bubaња et al., “Center-of-mass energy dependence of intrinsic- k_T distributions obtained from Drell–Yan production”, *Eur. Phys. J. C* **85** (2025) 278, arXiv:2404.04088.
- [7] I. Bubaња et al., “The small k_T region in Drell–Yan production at next-to-leading order with the parton branching method”, *Eur. Phys. J. C* **84** (2024) 154, arXiv:2312.08655.
- [8] S. Baranov et al., “CASCADE3 A Monte Carlo event generator based on TMDs”, *Eur. Phys. J. C* **81** (2021) 425, arXiv:2101.10221.
- [9] C. Bierlich et al., “A comprehensive guide to the physics and usage of PYTHIA 8.3”, *SciPost Phys. Codeb.* **2022** (2022) 8, arXiv:2203.11601.
- [10] T. Sjöstrand et al., “An introduction to PYTHIA 8.2”, *Comput. Phys. Commun.* **191** (2015) 159, arXiv:1410.3012.
- [11] A. Bermudez Martinez et al., “Collinear and TMD parton densities from fits to precision DIS measurements in the parton branching method”, *Phys. Rev. D* **99** (2019) 074008, arXiv:1804.11152.
- [12] J. Alwall et al., “The automated computation of tree-level and next-to-leading order differential cross sections, and their matching to parton shower simulations”, *JHEP* **1407** (2014) 079, arXiv:1405.0301.
- [13] H. Yang et al., “Back-to-back azimuthal correlations in Z+jet events at high transverse momentum in the TMD parton branching method at next-to-leading order”, *Eur. Phys. J. C* **82** (2022) 755, arXiv:2204.01528.
- [14] A. Bermudez Martinez et al., “The transverse momentum spectrum of low mass Drell–Yan production at next-to-leading order in the parton branching method”, *Eur. Phys. J. C* **80** (2020) 598, arXiv:2001.06488.
- [15] A. Bermudez Martinez et al., “Production of Z-bosons in the parton branching method”, *Phys. Rev. D* **100** (2019) 074027, arXiv:1906.00919.
- [16] A. Bermudez Martinez et al., “The transverse momentum spectrum of low mass Drell–Yan production at next-to-leading order in the parton branching method”, *Eur. Phys. J. C* **80** (2020) 598, arXiv:2001.06488.
- [17] D. Subotić, H. Jung, and N. Raičević, “Validation of the PB Framework in PYTHIA via Drell-Yan Production at NLO”, in “*Proceedings of QCD at the Extremes - PoS (QCDEX2025)*”, volume 508, p. 008. 2025.

- [18] J. O. Gonzalez-Hernandez, T. C. Rogers, and N. Sato, "Combining nonperturbative transverse momentum dependence with TMD evolution", *Phys. Rev. D* **106** (2022) 034002, arXiv:2205.05750.
- [19] CMS Collaboration, "Measurement of the mass dependence of the transverse momentum of lepton pairs in Drell-Yan production in proton-proton collisions at $\sqrt{s} = 13$ TeV", *Eur. Phys. J. C* **83** (2023) 628, arXiv:2205.04897.
- [20] N. Raičević, "Non-Perturbative Contributions to Low Transverse Momentum Drell-Yan Pair Production Using the Parton Branching Method", in *13th International Conference on New Frontiers in Physics*, Phys. Scr. 100 045306 (2025). arXiv:2412.00892.
- [21] G. Moreno et al., "Dimuon production in proton - copper collisions at $\sqrt{s} = 38.8$ GeV", *Phys. Rev. D* **43** (1991) 2815.
- [22] PHENIX Collaboration, "Measurements of $\mu\mu$ pairs from open heavy flavor and Drell-Yan in $p + p$ collisions at $\sqrt{s} = 200$ GeV", *Phys. Rev. D* **99** (2019) 072003, arXiv:1805.02448.
- [23] CDF Collaboration, "Transverse momentum cross section of e^+e^- pairs in the Z -boson region from $p\bar{p}$ collisions at $\sqrt{s} = 1.96$ TeV", *Phys. Rev. D* **86** (2012) 052010, arXiv:1207.7138.
- [24] J. M. Cornwall, "Dynamical Mass Generation in Continuum QCD", *Phys. Rev. D* **26** (1982) 1453.
- [25] O. Oliveira and P. Bicudo, "Running Gluon Mass from Landau Gauge Lattice QCD Propagator", *J. Phys. G* **38** (2011) 045003, arXiv:1002.4151.
- [26] P. Bicudo, O. Oliveira, P. J. Silva, and N. Cardoso, "Gluon mass at finite temperature in Landau gauge", *PoS LATTICE2013* (2014) 368, arXiv:1401.6289.
- [27] A. C. Aguilar, D. Binosi, and J. Papavassiliou, "Renormalization group analysis of the gluon mass equation", *Phys. Rev. D* **89** (2014) 085032, arXiv:1401.3631.
- [28] A. Deur, S. J. Brodsky, and C. D. Roberts, "QCD running couplings and effective charges", *Prog. Part. Nucl. Phys.* **134** (2024) 104081, arXiv:2303.00723.
- [29] D. V. Shirkov and I. L. Solovtsov, "Analytic model for the QCD running coupling with universal $\alpha_s(0)$ value", *Phys. Rev. Lett.* **79** (1997) 1209, arXiv:hep-ph/9704333.
- [30] I. L. Solovtsov and D. V. Shirkov, "The analytic approach in quantum chromodynamics", *Theor. Math. Phys.* **120** (1999) 1220, arXiv:hep-ph/9909305.
- [31] A. P. Bakulev, S. V. Mikhailov, and N. G. Stefanis, "QCD analytic perturbation theory: From integer powers to any power of the running coupling", *Phys. Rev. D* **72** (2005) 074014, arXiv:hep-ph/0506311.
- [32] A. V. Kotikov and I. A. Zemlyakov, "About Fractional Analytic QCD beyond Leading Order", in *International Workshop on Elementary Particles and Nuclear Physics. 7, 2022*. arXiv:2207.01330.

- [33] A. V. Kotikov and I. A. Zemlyakov, “Fractional analytic QCD beyond leading order”, *J. Phys. G* **50** (2023) 015001, arXiv:2203.09307.
- [34] A. V. Kotikov and I. A. Zemlyakov, “Fractional analytic QCD beyond leading order in the timelike region”, *Phys. Rev. D* **107** (2023) 094034, arXiv:2302.12171.
- [35] A. Deur, “The QCD Running Coupling”, arXiv:2502.06535.
- [36] Proceedings of Science (PoS), “Proceedings of Workshop QCD at the Extremes”. QCDEX2025, Dec, 2025.
- [37] M. A. Braun, “Reggeized gluons with a running coupling constant”, *Phys. Lett. B* **348** (1995) 190–195, arXiv:hep-ph/9408261.
- [38] ATLAS Collaboration, “Determination of the strong coupling constant from transverse energy–energy correlations in multijet events at $\sqrt{s} = 13$ TeV with the ATLAS detector”, *JHEP* **07** (2023) 085, arXiv:2301.09351.
- [39] Flavour Lattice Averaging Group (FLAG) Collaboration, “FLAG Review 2021”, *Eur. Phys. J. C* **82** (2022) 869, arXiv:2111.09849.
- [40] Particle Data Group Collaboration, “Review of Particle Physics”, *PTEP* **2022** (2022) 083C01.
- [41] D. Britzger et al., “Calculations for deep inelastic scattering using fast interpolation grid techniques at NNLO in QCD and the extraction of α_s from HERA data”, *Eur. Phys. J. C* **79** (2019) 845, arXiv:1906.05303. [Erratum: *Eur.Phys.J.C* 81, 957 (2021)].
- [42] S. Narison, “ $\alpha_s(\mu)$ from $M_{\chi_{0c(0b)}} - M_{\eta_{c(b)}}$ @N2LO”, in *21st High-Energy Physics International Conference in Quantum Chromodynamics*. 12, 2018. arXiv:1812.09360.
- [43] ATLAS Collaboration, “Measurement of dijet azimuthal decorrelations in pp collisions at $\sqrt{s} = 8$ TeV with the ATLAS detector and determination of the strong coupling”, *Phys. Rev. D* **98** (2018) 092004, arXiv:1805.04691.
- [44] D. Boito et al., “Strong coupling from $e^+e^- \rightarrow$ hadrons below charm”, *Phys. Rev. D* **98** (2018) 074030, arXiv:1805.08176.
- [45] ATLAS Collaboration, “Determination of the strong coupling constant α_s from transverse energy–energy correlations in multijet events at $\sqrt{s} = 8$ TeV using the ATLAS detector”, *Eur. Phys. J. C* **77** (2017) 872, arXiv:1707.02562.
- [46] H1 Collaboration, “Determination of the strong coupling constant $\alpha_s(m_Z)$ in next-to-next-to-leading order QCD using H1 jet cross section measurements”, *Eur. Phys. J. C* **77** (2017) 791, arXiv:1709.07251. [Erratum: *Eur.Phys.J.C* 81, 738 (2021)].
- [47] CMS Collaboration, “Measurement and QCD analysis of double-differential inclusive jet cross sections in pp collisions at $\sqrt{s} = 8$ TeV and cross section ratios to 2.76 and 7 TeV”, *JHEP* **03** (2017) 156, arXiv:1609.05331.
- [48] T. Klijnsma, S. Bethke, G. Dissertori, and G. P. Salam, “Determination of the strong coupling constant $\alpha_s(m_Z)$ from measurements of the total cross section for top-antitop quark production”, *Eur. Phys. J.* **C77** (2017) 778, arXiv:1708.07495.

- [49] CMS Collaboration, “Constraints on parton distribution functions and extraction of the strong coupling constant from the inclusive jet cross section in pp collisions at $\sqrt{s} = 7$ TeV”, *Eur. Phys. J. C* **75** (2015) 288, arXiv:1410.6765.
- [50] CMS Collaboration, “Measurement of the inclusive 3-jet production differential cross section in proton–proton collisions at 7 TeV and determination of the strong coupling constant in the TeV range”, *Eur. Phys. J. C* **75** (2015) 186, arXiv:1412.1633.
- [51] CMS Collaboration, “Measurement of the Ratio of the Inclusive 3-Jet Cross Section to the Inclusive 2-Jet Cross Section in pp Collisions at $\sqrt{s} = 7$ TeV and First Determination of the Strong Coupling Constant in the TeV Range”, *Eur. Phys. J. C* **73** (2013) 2604, arXiv:1304.7498.
- [52] JADE Collaboration, “Measurement of the strong coupling α_s from the three-jet rate in e^+e^- - annihilation using JADE data”, *Eur. Phys. J. C* **73** (2013), no. 3, 2332, arXiv:1205.3714.
- [53] D0 Collaboration, “Measurement of angular correlations of jets at $\sqrt{s} = 1.96$ TeV and determination of the strong coupling at high momentum transfers”, *Phys. Lett. B* **718** (2012) 56, arXiv:1207.4957.
- [54] OPAL Collaboration, “Determination of α_s using OPAL hadronic event shapes at $\sqrt{s} = 91 - 209$ GeV and resummed NNLO calculations”, *Eur. Phys. J. C* **71** (2011) 1733, arXiv:1101.1470.
- [55] D0 Collaboration, “Determination of the strong coupling constant from the inclusive jet cross section in $p\bar{p}$ collisions at $\sqrt{s} = 1.96$ TeV”, *Phys. Rev. D* **80** (2009) 111107, arXiv:0911.2710.
- [56] JADE Collaboration, “Determination of the Strong Coupling α_s from hadronic Event Shapes with $O(\alpha_s^3)$ and resummed QCD predictions using JADE Data”, *Eur. Phys. J. C* **64** (2009) 351, arXiv:0810.1389.
- [57] G. Dissertori et al., “Determination of the strong coupling constant using matched NNLO+NLLA predictions for hadronic event shapes in e^+e^- annihilations”, *JHEP* **08** (2009) 036, arXiv:0906.3436.
- [58] C. Glasman, “Precision measurements of α_s at HERA”, *AIP Conf. Proc.* **792** (2005) 689, arXiv:hep-ex/0506035.